doi:10.1246/cl.2011.1428
Published on the web December 3, 2011

Synthesis and Lithium Storage Properties of NiO@TiO_2 Nanotube Heterojunction Arrays

Lili Wang, Shichao Zhang,* and Xiaomeng Wu
School of Materials Science and Engineering, Beijing University of Aeronautics and Astronautics, Beijing 100191, P. R. China

(Received August 12, 2011; CL-110676; E-mail: csc@buaa.edu.cn)

The present work describes using TiO_2 nanotube arrays as the building block to form ordered NiO@TiO_2 heterojunctions via pulse electrodeposition and sequential annealing, and a key finding in the electrochemical investigation is that the enhanced capacity and rate capability derives from the hybrid nature of the electrodes with improved conductivity and dual lithium storage mechanism.

In the past decades, self-organized TiO_2 nanotube arrays have received considerable attention with respect to their dramatic physicochemical properties that could find potential applications in photocatalysis,[1] dye-sensitive solar cells,[2,3] lithium batteries,[4,5] gas sensors,[6,7] and so on. However, to fully exploit these unique nanotube arrays in applications such as energy conversion and storage, it is essential to devise new ways to functionalize the interior space. Among various solutions,[8–11] attachment of appropriate chemical functionalities on TiO_2 nanotubes could be an effective route for optimizing their physicochemical and electrochemical properties.

Recently, the complete filling of the interior region of TiO_2 nanotubes, which allows for the production of metallic nanowires for electronic or magnetic devices, has been reported.[12] Despite the potential advantages for application, the specific heterostructure would inevitably bring a significant drawback with respect to the block of vertical channel for mass transport. Therefore, a tube-in-tube nanostructure, constructed from a narrow inner tube within a host tube, exhibits multiple functionalities without harming the original tubular structure advantage and thus should be more competitive.

Herein, a novel NiO@TiO_2 nanocomposite with tube-in-tube structure is successfully fabricated via pulse electrodeposition and subsequent annealing, and the electrochemical lithium storage of the nanocomposite is investigated on the basis of improving specific capacity and rate capability.

Self-organized TiO_2 nanotube arrays were fabricated via anodic oxidation of Ti foil in the electrolyte of ethylene glycol containing 0.25 wt % NH_4F and 2 vol % H_2O.[13,14] The as-prepared TiO_2 nanotube arrays were then heat-treated at 450 °C in air for 1 h to convert amorphous TiO_2 into crystalline form. After that, pulse electrodeposition was performed on a PARSTAT 2273 electrochemical workstation under a three-electrode system with TiO_2 nanotubes immersing in the electrolyte water bath containing 0.1 mol L^{-1} $NiCl_2 \cdot 6H_2O$, 0.6 mol L^{-1} $Ni_2SO_4 \cdot 6H_2O$, and 0.3 mol L^{-1} H_3BO_3 at 30 °C. Pulse currents were adopted with anode current 0 mA cm^{-2} lasting 250 ms and −100 mA cm^{-2} as cathode current for 25 ms. Subsequently, the successfully prepared electrode was annealed at 500 °C in air for 90 min to oxidize the metallic Ni into NiO.

The crystal structures of both Ni@TiO_2 and NiO@TiO_2 nanotube arrays were examined by X-ray diffraction (XRD; Cu Kα radiation) while the morphology and microstructure were characterized by scanning electron microscopy (SEM) and transmission electron microscopy (TEM). Cyclic voltammetric (CV) measurement was performed on an IM6ex Workstation within the potential range between −3.5 and 3 V at a scan rate of 5 mV s^{-1}.

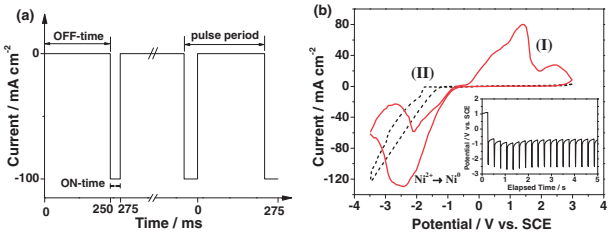

Figure 1. (a) A typical pulse-current waveform with anode current (0 mA cm^{-2}, 250 ms) and cathode current (−100 mA cm^{-2}, 25 ms). (b) Cyclic voltammograms of pristine TiO_2 nanotubes immersed in (I) prepared Ni^{2+}-containing electrodeposition electrolyte, (II) 1 mol L^{-1} Na_2SO_4 solution, and selected potential–time curve of electrodeposition process (inset).

Cells were assembled in an argon-filled glove box with NiO@TiO_2 nanotube arrays as working electrode, metallic Li sheet as reference and counter electrodes, polypropylene (PP) film as separator, and 1 M $LiPF_6$ in a 1:1 mixture of EC and DEC as electrolyte. Rate capabilities were studied using various current densities. CV measurements were also conducted within the potential range between 0 and 3 V at a scan rate of 0.2 mV s^{-1}.

The typical pulse-current waveform applied in our experiment is shown in Figure 1a. The ON-time and OFF-time constitute one pulse period. According to the CV measurement discussed in the following section, the cathode current at −100 mA cm^{-2} was applied to deposit metallic Ni. The anode current of 0 mA cm^{-2} aimed to discharge the capacitance of the barrier layer and promptly replenishing metal ions in the diffusion layer.[15] It is notable that enhancing the conductivity of TiO_2 is necessary for conducting the deposition effectively. In the current case, electrochemical reduction is a feasible way to tune the doping level of TiO_2, which is accompanied by a charge compensation via proton intercalation ($Ti^{4+} + e^- + H^+ \rightarrow Ti^{3+}H^+$).[12] Consequently, the deposition of Ni could take place simultaneously with the self-doping of TiO_2.

CVs were carried out for choosing the optimal parameters for the deposition. Curve I in Figure 1b belongs to the CV of TiO_2 nanotubes tested in Ni^{2+}-containing deposition electrolyte. In order to exclude the impact of hydrogen evolution and ascertain the Ni deposition potential, pristine TiO_2 nanotubes were intentionally tested in 1 mol L^{-1} Na_2SO_4 solution for comparison (curve II). Evidently, hydrogen evolution occurs

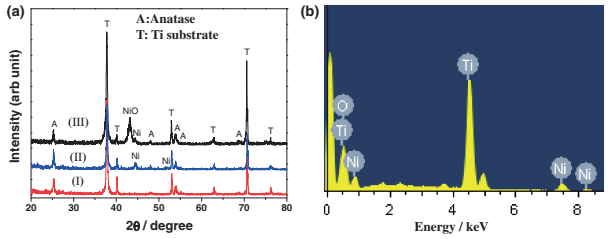

Figure 2. (a) XRD patterns of (I) pristine TiO_2 nanotubes, (II) Ni@TiO_2 nanotubes fabricated by pulse electrodeposition, and (III) NiO@TiO_2 nanotubes annealed at 500 °C for 90 min in air after electrodeposition. (b) EDX analysis of NiO@TiO_2 nanotube arrays.

continuously at more negative potentials, and the cathode peak located at −2.4 V should be attributed to the reduction of Ni^{2+} to Ni^0; the corresponding peak current of deposition is about 130 mA cm^{-2}. Accordingly, the inset of Figure 1b illustrates the actual curve in pulse deposition model, and the parameters are close to the values obtained by CV.

XRD patterns of the obtained samples are shown in Figure 2. Strong peaks at 37.8, 53, and 70.6° are indexed to substrate Ti, and the two obvious peaks at around 25 and 48° are ascribed to TiO_2. After deposition, metallic Ni was embedded into TiO_2 nanotubes, and its corresponding peaks appear at 44.6 and 51.9°. In pattern III, the peak located at 43.2° can be indexed to NiO phase. The energy dispersive X-ray (EDX) analysis of Ni@TiO_2 nanotube arrays in Figure 2b further confirms the existence of elemental Ni with a weight ratio of 4.35 wt %.

The FESEM images of TiO_2 nanotube arrays before and after deposition are illustrated in Figure 3. Figure 3a depicts the general view of as-prepared TiO_2 nanotube arrays which are uniformly and vertically grown on Ti foil substrate. The tube is approximately 120 nm in diameter and 6.5 μm in length. During the deposition, metallic Ni grew well from the bottom of the interior wall up to top surface with upright morphology. Meanwhile, the hollow tubular TiO_2 structure provided structural supports and constituted the exterior part of the overall structure. After deposition, the Ni@TiO_2 nanotube arrays present a tube-in-tube structure, as seen in Figure 3b. The inset of Figure 3b manifests the NiO@TiO_2 nanotube arrays after annealing, which keep the good tube-in-tube architecture and nearly have no modifications in morphology.

The formation of the nickel-based continuous and uniform tubular structure was further verified by TEM examination. Clearly, a distinct boundary between the double-layer nanotube arrays can be observed in Figure 3c, and the distribution and the wall thickness of the deposited Ni nanotube is uniform, which indicate the deposition initiated from inner surfaces of the cup-shaped nanotubes simultaneously (inset). As indicated by Figure 3d, the outer TiO_2 layer is approximately 18 nm in thickness and the inner NiO layer 20 nm. It also demonstrates that the subsequent heat treatment did not lead to the collapse or deformation of nickel-based nanotubes and that the well-defined nanotubular structure can maintain very well. Moreover, the selected area electron diffraction pattern (SAED) image, inset Figure 3d, presents the polycrystalline (presence of both anatase and bunsenite) nature of the materials due to the spot and ring patterns.

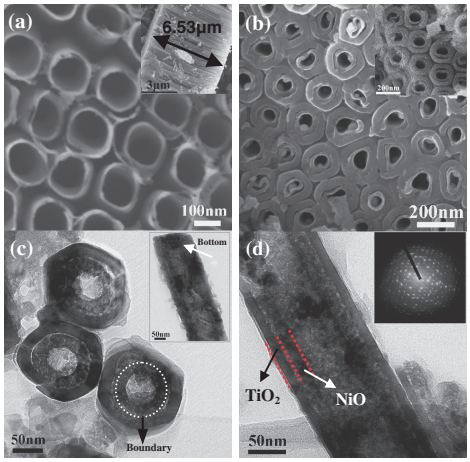

Figure 3. FESEM images of (a) top view and cross-section (inset) of as-prepared TiO_2 nanotubes, (b) Ni@TiO_2 nanotubes after electrodeposition and the inset of NiO@TiO_2 nanotubes after annealing. TEM images of (c) cross-section of Ni@TiO_2 nanotubes and single Ni@TiO_2 nanotube (inset), (d) single NiO@TiO_2 nanotube and SAED (inset).

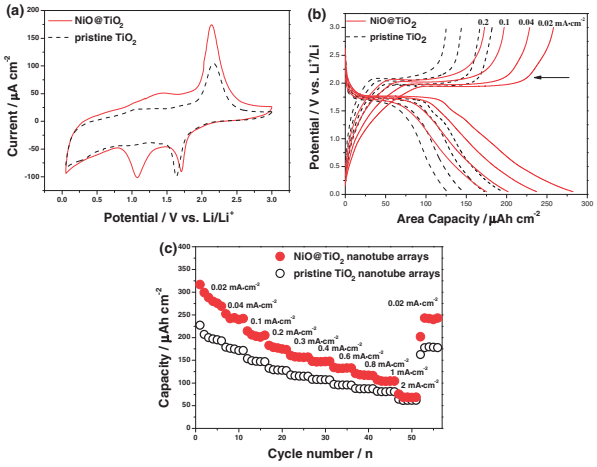

Figure 4. (a) Cyclic voltammograms of NiO@TiO_2 and pristine TiO_2 nanotube arrays with a scan rate of 0.2 mV s^{-1} in a potential range between 0 and 3 V. (b) Voltage–area capacity profiles at different current densities and (c) rate cycling performance for NiO@TiO_2 and pristine TiO_2 nanotube arrays between the voltage ranges of 0.05 and 3 V.

The electrochemical performances of both NiO@TiO_2 and pristine TiO_2 nanotube arrays as anode materials were investigated in Figure 4. Figure 4a shows the cyclic voltammogram curves. The typical pair of peaks located at ca. 1.75 and ca. 2.0 V vs. Li^+/Li is attributed to the TiO_2, corresponding to the lithium insertion and extraction behavior from tetrahedral and octahedral sites of anatase lattice respectively (eq 1). In addition, the peaks at ca. 1.2 and ca. 1.45 V are related to the redox reaction of NiO. Accordingly, the overall reversible reaction mechanisms for NiO@TiO_2 nanocomposite can be described as:

$$TiO_2 + xLi^+ + xe^- \rightleftharpoons Li_xTiO_2 \ (0 \le x \le 1) \quad (1)$$

$$NiO + 2Li^+ + 2e^- \rightleftharpoons Li_2O + Ni \quad (2)$$

As mentioned above, the extra redox peaks in Figure 4a correspond to the mechanism of Li reactivity for NiO. The cathodic peak located at 1.2 V is ascribed to the reduction of NiO into metallic Ni and the formation of amorphous Li_2O and the solid electrolyte interphase (SEI). In the anodic scan, the broad peaks at 1.45 and 2.2 V (overlapped with TiO_2 anodic peak) are consistent with the oxidation of NiO and decomposition of Li_2O and the SEI.[16]

Figure 4b shows the charge/discharge curves at different current densities of 0.02, 0.04, 0.1, and 0.2 mA cm^{-2}. During the charge/discharge process, voltage plateaus located at around 1.75 and 2 V are attributed to Li^+ insertion/extraction in crystalline TiO_2 nanotubes. As the current density increases, the voltage plateaus become much shorter and the voltage differences become wider, both to pristine TiO_2 and NiO@TiO_2 nanotube arrays. Actually, the fast kinetics shortens the charge/discharge time, and Li^+ ions may possibly not have sufficient time to insert into or extract from the nanotubular matrix. In addition, NiO@TiO_2 delivers a much higher capacity and longer voltage plateau than pristine TiO_2 at the same current density. Intrinsically, plausible mechanisms for the contributions of Ni to the capacity are elucidated as follows: (1) the increased defect sites caused by Ti ions between the TiO_2 and Ni layer were partially reduced from Ti^{4+} to Ti^{3+}/Ti^{2+} under annealing, leading to an oxygen-deficient environment at the interface which may indicate a slight increase in the electronic conductivity of the TiO_2, thereby inducing the formation of favorable electron transport;[17] (2) the residual metallic Ni after annealing and metallic Ni formed during discharge would also contribute to the increase of electronic conductivity and be beneficial to the electrochemical reaction activity of the nanocomposite.[18]

Rate capacities dependent on cycle numbers are shown in Figure 4c. Different current densities ranging from 0.02 to 2 mA cm^{-2} are applied. At the current density of 0.02 mA cm^{-2}, pristine TiO_2 delivers a capacity of only 199.8 μA h cm^{-2} while NiO@TiO_2 up to 280.02 μA h cm^{-2}, with an elevation of 40% in capacity. When current density rise to 0.2 mA cm^{-2}, their capacities are 128.5 and 176.95 μA h cm^{-2} respectively, keeping the capacity elevation of 38%. Actually, to some extent, there is always an obvious increase for NiO@TiO_2 in capacity compared to pristine TiO_2 at different kinetics. Furthermore, with the current density shifts from 0.02 mA cm^{-2} up to high rate of 0.2 mA cm^{-2}, 63% of capacity retention still remains for NiO@TiO_2 nanotube arrays. When back to the initial 0.02 mA cm^{-2}, the electrode almost reassumes the original capacity (approximately 192 μA h cm^{-2}), this being another confirmation of the exceptional capability of this electrode to keep its integrity not only for a long number of cycles but also at high rates.

Generally speaking, the total stored charges (Li^+) in the films are strongly dependent on the charge/discharge rates. As the rate increases, the total amount of stored charges decreases. This indicates that full storage capacity could not been reached at the given rate because of kinetic limitations associated with the diffusion of Li^+ through the active materials. That is, the decreasing capacity with increasing current rate is most probably due to limited lithium diffusion; namely, the Li^+ could only diffuse and intercalate into a certain depth of the materials at high rates. Besides, the poor conductivity at high rates also restricts the electron transport and diffusion.

In summary, we have successfully fabricated novel NiO@TiO_2 nanotube arrays with a tube-in-tube structure. Besides, electrochemical tests manifest that this new material has excellent advantages in cycling performance and rate capability. Combining the merits of high aspect ratio and convenience for ion transport, NiO@TiO_2 nanotube arrays are promising and desirable anode materials for lithium-ion batteries. More importantly, the synthetic method presented here may also provide a general strategy for the fabrication of other inorganic tube-in-tube nanostructures.

Financial supports from National Basic Research Program of China (No. 2007CB936502) and National Natural Science Foundation of China (Nos. 50954005 and 51074011) are greatly appreciated.

References

1 M. Zlamal, J. M. Macak, P. Schmuki, J. Krýsa, *Electrochem. Commun.* **2007**, *9*, 2822.
2 G. K. Mor, K. Shankar, M. Paulose, O. K. Varghese, C. A. Grimes, *Nano Lett.* **2006**, *6*, 215.
3 S. H. Kang, J.-Y. Kim, Y. Kim, H. S. Kim, Y.-E. Sung, *J. Phys. Chem. C* **2007**, *111*, 9614.
4 G. F. Ortiz, I. Hanzu, T. Djenizian, P. Lavela, J. L. Tirado, P. Knauth, *Chem. Mater.* **2009**, *21*, 63.
5 M. Mancini, P. Kubiak, J. Geserick, R. Marassi, N. Hüsing, M. Wohlfahrt-Mehrens, *J. Power Sources* **2009**, *189*, 585.
6 H. F. Lu, F. Li, G. Liu, Z.-G. Chen, D.-W. Wang, H.-T. Fang, G. Q. Lu, Z. H. Jiang, H.-M. Cheng, *Nanotechnology* **2008**, *19*, 405504.
7 Q. Zheng, B. Zhou, J. Bai, L. Li, Z. Jin, J. Zhang, J. Li, Y. Liu, W. Cai, X. Zhu, *Adv. Mater.* **2008**, *20*, 1044.
8 L. Xue, Z. Wei, R. Li, J. Liu, T. Huang, A. Yu, *J. Mater. Chem.* **2011**, *21*, 3216.
9 Y. Xie, L. Zhou, C. Huang, H. Huang, J. Lu, *Electrochim. Acta* **2008**, *53*, 3643.
10 S. K. Mohapatra, S. Banerjee, M. Misra, *Nanotechnology* **2008**, *19*, 315601.
11 Y. Zhang, Y. Yang, P. Xiao, X. Zhang, L. Lu, L. Li, *Mater. Lett.* **2009**, *63*, 2429.
12 J. M. Macak, B. G. Gong, M. Hueppe, P. Schmuki, *Adv. Mater.* **2007**, *19*, 3027.
13 D. Gong, C. A. Grimes, O. K. Varghese, W. Hu, R. S. Singh, Z. Chen, E. C. Dickey, *J. Mater. Res.* **2001**, *16*, 3331.
14 X. Wu, Y. Ling, L. Liu, Z. Huang, *J. Electrochem. Soc.* **2009**, *156*, K65.
15 M. S. Chandrasekar, M. Pushpavanam, *Electrochim. Acta* **2008**, *53*, 3313.
16 X. H. Huang, J. P. Tu, B. Zhang, C. Q. Zhang, Y. Li, Y. F. Yuan, H. M. Wu, *J. Power Sources* **2006**, *161*, 541.
17 H. S. Kim, S. H. Kang, Y. H. Chung, Y.-E. Sung, *Electrochem. Solid-State Lett.* **2010**, *13*, A15.
18 L. P. An, X. P. Gao, G. R. Li, T. Y. Yan, H. Y. Zhu, P. W. Shen, *Electrochim. Acta* **2008**, *53*, 4573.

